Research Article

Abdullah R. Alzahrani, Ibrahim Abdel Aziz Ibrahim*, Ibrahim M. Alanazi, Naiyer Shahzad, Imran Shahid, Mohd Fahami Nur Azlina, Yusof Kamisah, Nafeeza Mohd Ismail, and Palanisamy Arulselvan

Graphene oxide/chitosan/manganese/folic acid-brucine functionalized nanocomposites show anticancer activity against liver cancer cells

https://doi.org/10.1515/gps-2023-0184
received September 15, 2023; accepted January 15, 2024

Abstract: Nanomedicine is the application of nanomaterials and nanotechnology to the development of novel pharmaceuticals and drug delivery mechanisms. The present study synthesized a functionalized nanocomposite (NC) containing graphene oxide (GO), chitosan (Ch), manganese (Mn), folic acid (FA), and brucine. The anticancer properties of the synthesized GO/Mn/Ch/FA-Brucine NCs were evaluated against liver cancer cells. GO/Mn/Ch/FA-Brucine NCs were characterized using several characterization techniques. The growth of HepG2 and Hep3B cells was analyzed using the methylthiazolyldiphenyl-tetrazolium bromide assay. The cell apoptosis was examined through dual staining. The levels of inflammatory and oxidative stress biomarkers were measured using the corresponding assay kits. Various characterization assays revealed the formation of crystalline GO/Mn/Ch/FA-Brucine NCs with tetragonal and agglomerated morphologies, various stretching and bonding, and an average particle size of 136.20 nm. GO/Mn/Ch/FA-Brucine NCs have effectively inhibited the viabilities of HepG2 and Hep3B cells. The NCs increased thiobarbituric acid reactive substances and reduced antioxidants and inflammatory mediators, thereby promoting apoptotic cell death in HepG2 cells. Our findings indicate that GO/Mn/Ch/FA-Brucine NCs can inhibit viability and promote apoptosis in liver cancer HepG2 cells.

Keywords: liver cancer, nanocomposites, apoptosis, Brucine, chitosan, oxidative stress

1 Introduction

Liver cancer is the third major cause of mortality worldwide, despite extensive research efforts devoted to its treatment. The prevalence of this disease is higher among males than females [1,2]. A report submitted to the World Health Organization by the International Agency for Research on Cancer has included the findings on the global incidence of liver cancer in the year 2020, indicating that a total of 905,700 individuals were diagnosed with this disease, and out of this diagnosed population, 830,200 individuals died due to liver cancer. According to the reports, it was projected that the incidence and mortality rates of liver cancer may increase by 55% by the year 2040 [3,4]. The major problem with treating liver cancer is that it is usually identified at a late stage. Therapeutic procedures, such as resection or transplantation, can be applied only to a small percentage of patients [5]. In order to address the limitations of current techniques, there is an ongoing pursuit to identify new anticancer drugs that exhibit enhanced efficacy while minimizing adverse effects. Several targeted therapeutics have been identified for the management of liver cancer; nevertheless, their effectiveness against cancer cells has been limited [6].

Nanocomposite (NC) materials consist of many phases, each exhibiting dimensions at the nanoscale ranging from one to three nanometers. The understanding of the relationship between structure and property is significantly impacted by the proportion of surface area to volume of the material employed in the formulation of NCs [7]. NCs offer a plethora of innovative solutions for tackling challenges across diverse

* **Corresponding author: Ibrahim Abdel Aziz Ibrahim**, Department of Pharmacology and Toxicology, Faculty of Medicine, Umm Al-Qura University, Makkah, Saudi Arabia, e-mail: iamustafa@uqu.edu.sa
Abdullah R. Alzahrani, Ibrahim M. Alanazi, Naiyer Shahzad, Imran Shahid: Department of Pharmacology and Toxicology, Faculty of Medicine, Umm Al-Qura University, Makkah, Saudi Arabia
Mohd Fahami Nur Azlina, **Yusof Kamisah:** Department of Pharmacology, Faculty of Medicine, Universiti Kebangsaan Malaysia, Kuala Lumpur, Malaysia
Nafeeza Mohd Ismail: Department of Pharmacology, Faculty of Medicine, Universiti Teknologi MARA, Sungai Buloh Campus, Selangor, Malaysia
Palanisamy Arulselvan: Department of Chemistry, Saveetha School of Engineering, Saveetha Institute of Medical and Technical Sciences (SIMATS), Saveetha University, Chennai, Tamil Nadu, 602 105, India

sectors such as medicine, foods and beverages, and electronics. The physical attributes of the nanocrystals possess potential usage in the advancement of new and potential sensors for tumor detection, tumor imaging, and pharmaceuticals for cancer treatment [8].

Ch, a naturally occurring polysaccharide, is commonly present in certain seafood types, including shrimp, crab, and crayfish, with the highest concentration found in their shells. Ch possesses several key characteristics, namely biocompatibility, biodegradability, and non-toxicity [9,10]. Graphene oxide (GO) exhibits hydrophilic properties and high dispensability in aqueous and organic solvents because of the occurrence of oxygen-containing functional groups [11]. Due to its distinctive properties, GO exhibits significant promise in the fields of nanomedicine and biomedical applications [12]. GO has been the subject of study in the area of drug delivery due to its significant hydrophobic surface area, which facilitates the loading of hydrophobic medicines through non-covalent adsorption [13]. The large surface area of GO and the existence of oxygenated functional groups facilitate the implementation of several techniques for modifying nanomaterials. These techniques include chemical functionalization and the application of molecules and polymers as coatings. These modifications are employed to design drug delivery systems [14].

In the context of functionalization, GO exhibits a notable benefit compared to other nanocarriers. This advantage primarily relies on the abundant occurrence of carboxylic groups, which facilitates the coupling of several molecules compared to other nanocarriers like liposomes and solid lipid nanoparticles. Furthermore, it has been observed that an increased level of functionalization of GO can enhance the functionality of the nanocarrier [15]. Brucine is a major bioactive compound derived from the *Strychnos nux vomica* L. seeds [16]. Several earlier studies have already revealed that brucine demonstrated anticancer properties against various cancers [17–19]. The synthesis of GO-functionalized chitosan (Ch)-brucine NCs and their biological activities have not been reported yet. Therefore, the current study aims at synthesizing and characterizing the GO, Ch, manganese, brucine, and folic acid (FA) functionalized NCs (GO/Mn/Ch/FA-Brucine NCs) and evaluating their anticancer potentials against liver cancer cells.

2 Materials and methods

2.1 Chemicals and reagents

The following chemicals, including GO, manganese nitrate, Ch, FA, and brucine ($C_{23}H_{26}N_2O_4$), were purchased from Sigma-Aldrich, USA. All assay kits to determine the biochemical parameters were acquired from Thermofisher and eBioscience, USA.

2.2 Synthesis of GO/Mn/Ch/FA-Brucine NCs

In 50 mL of distilled water, 500 mg of synthetic GO and 0.1 M of manganese(II) nitrate hexahydrate ($Mn(NO_3)_2{\cdot}6H_2O$) were dissolved. The solution was then supplemented with 50 mL of distilled water, 0.5 g of Ch, and 1% acetic acid. To this mixture, 50 mg of brucine was added, followed by 100 mg of FA. NaOH (0.1 M) was then introduced drop-by-drop, and the suspension was heated with magnetic stirring for 6 h at 60°C. The resultant nanopowder was rinsed with ethanol and distilled water. To formulate GO/Mn/Ch/FA-Brucine NCs, we dried the precipitate at 120°C for 1 h, followed by annealing of the nanopowder at 200°C for 2 h.

2.3 Characterization of GO/Mn/Ch/FA-Brucine NCs

The UV-vis spectrophotometer (Shimadzu-1700, Japan) was used to analyze the synthesized GO/Mn/Ch/FA-Brucine NCs. The spectral characteristics of the NCs were analyzed within the wavelength range of 100–1,000 nm.

GO/Mn/Ch/FA-Brucine NCs were subjected to photoluminescence (PL) analysis using PL spectroscopy (F-2500 FL, Hitachi).

The X-ray diffraction (XRD) analysis was performed using the X'pert Pro PANalytical XRD machine. The NCs were examined and scanned for 0.02–0.5 s and a voltage of 40 kV and 45 mA.

The Fourier-transform infrared spectroscopy (FT-IR) study was conducted to investigate the stretching and bonding present in GO/Mn/Ch/FA-Brucine NCs. The NCs were analyzed using the Shimadzu-8400S (Japan) equipment. A spectrum of the NCs was acquired using the KBr disc technique at 4,000–500 cm^{-1}.

The elemental profile of the NCs was analyzed using energy-dispersive X-ray spectroscopy (EDX), whereas their morphology and spatial distribution were analyzed using scanning electron microscopy (SEM) (Carl Zeiss Ultra 55 FESEM).

The transmission electron microscopy (TEM) analysis was conducted to examine the size and morphology of the NCs (TECNAI F30, USA). The copper grid holding the NCs was subjected to electronic radiation within a vacuum environment. Images of the samples were obtained using an electron beam.

The distribution and size of the NCs were examined using the Zeta sizer (Malvern, USA) dynamic light scattering (DLS) apparatus.

2.4 Antimicrobial activity

The well diffusion technique was employed to examine the antibacterial property of GO/Mn/Ch/FA-Brucine NCs against various pathogens, including *Bacillus subtilis*, *Staphylococcus aureus*, *Proteus vulgaris*, *Klebsiella pneumoniae*, *Streptococcus pneumoniae*, *Escherichia coli*, and *Candida albicans* [20]. Each strain was grown on an appropriate agar growth medium. Following the inoculation, the wells were developed on the agar surface using a sterile cork borer. Subsequently, the NCs were introduced into the wells at concentrations of 1, 1.5, and 2 $\mu g \cdot mL^{-1}$. The plates were incubated for 24 h, and the inhibitory zone diameter was then noted. Amoxicillin was used as a positive control.

2.5 Cell collection and maintenance

The liver cancer HepG2 and Hep-3B cells were collected from the ATCC, USA. Subsequently, the cells were grown in a CO_2 incubator at 37°C, using Dulbecco's modified eagle medium with 10% fetal bovine serum and 1% antimycotic mixtures. Upon reaching 80% confluency, the cells were subjected to trypsinization and used for further assays.

2.6 MTT assay

The assessment of HepG2 and Hep3B cell viability following treatment with GO/Mn/Ch/FA-Brucine NCs was conducted using the methylthiazolyldiphenyl-tetrazolium bromide assay [21]. Both cells were cultured separately in 96-well plates at a cell population of 5×10^3 cells/well for 24 h. Later, the cells were exposed to varying doses of the NCs (2, 4, 6, 8, 10, and 12 µg) for 24 h. Approximately 20 µL of MTT reagent was introduced to each well and incubated for 4 h. The developed formazan deposits were subsequently liquefied in 100 µL of dimethyl sulfoxide, and the absorbance was recorded at 570 nm.

2.7 Dual staining

The dual staining technique [22] was used to assay the apoptotic cell death in HepG2 cells following treatment with GO/Mn/Ch/FA-Brucine NCs. The cells were grown on a 24-well plates for 24 h, with a cell population of 5×10^5 cells/well. The NCs were subsequently treated at concentrations of 6 and 8 µg for 24 h. Later, the cells were stained using acridine orange/ethidium bromide) dye (100 $\mu g \cdot mL^{-1}$, 1:1 ratio) for 5 min. Following the staining process, the fluorescence intensity was assessed using a fluorescent microscope.

2.8 Quantification of oxidative stress markers

The concentrations of thiobarbituric acid reactive substances (TBARS) and the antioxidants (glutathione [GSH], superoxide dismutase [SOD], and catalase [CAT]) in the cell lysates of both untreated and NC-treated HepG2 cells were quantified using commercially available assay kits. These assays were performed according to the suggested protocols provided by the kit's manufacturer (ThermoFisher Scientific, USA).

2.9 Measurement of inflammatory marker levels

The levels of tumor necrosis factor alpha (TNF-α), nuclear factor Kappa-light-chain-enhancer of activated B cells (NF-κB), cyclooxygenase-2 (COX-2), and interleukin-6 (IL-6) in the cell lysates of both untreated and NC-treated HepG2 cells were measured using the assay kits. These assays were performed according to the suggested protocols provided by the kit's manufacturer (ThermoFisher Scientific, USA).

2.10 Statistical analysis

Dara are illustrated as the mean ± SD of three individual measurements, which were examined using the GraphPad Prism software. The values of the treatment groups were analyzed using one-way ANOVA and Duncan's multiple range test (DMRT) to measure significant variations, which was set at $p < 0.05$.

3 Results

3.1 Characterization of GO/Mn/Ch/FA-Brucine NCs

Figure 1a depicts the results of the UV-visible spectrum analysis for the synthesized GO/Mn/Ch/FA-Brucine NCs. The absorbance at several wavelengths (100–1,000 nm)

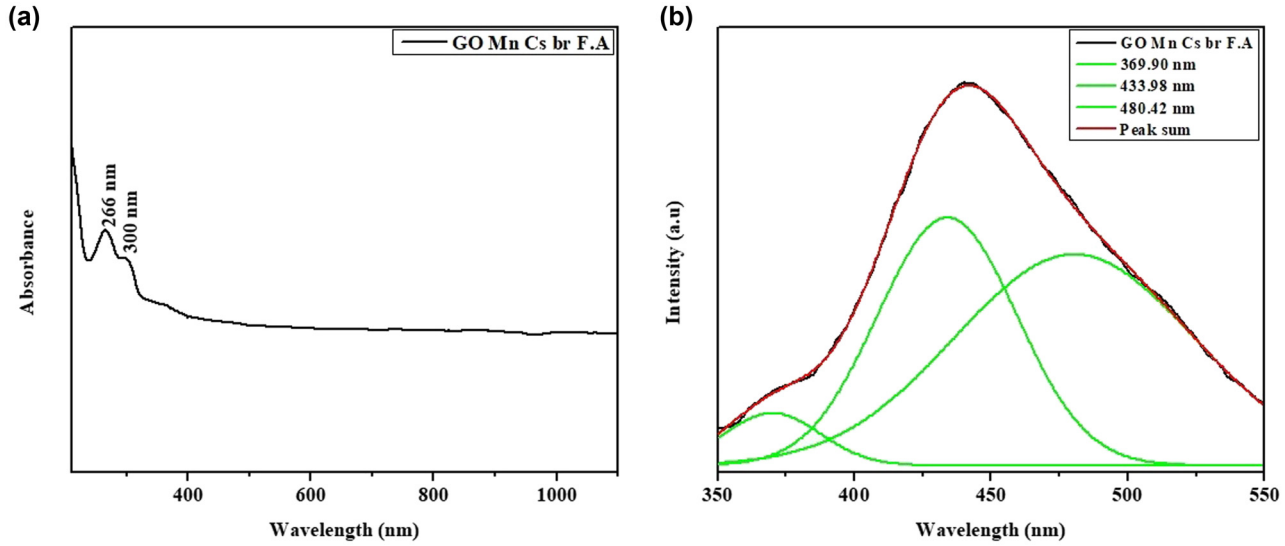

Figure 1: UV-visible spectroscopy and PL analysis of the synthesized GO/Mn/Ch/FA-Brucine NCs. The analysis of absorbance at several wavelengths (100–1,000 nm) revealed that the highest absorbance peak occurred at 266 and 300 nm (a). The wavelengths at which the excitations of the synthesized GO/Mn/Ch/FA-Brucine NCs occurred were determined to be 369.90, 433.98, and 480.42 nm, respectively, which reveals the crystal mode, surface characteristics, and structural flaws shown by the synthesized GO/Mn/Ch/FA-Brucine NCs (b).

revealed that the highest absorbance peaks occurred at 266 and 300 nm, verifying the NCs' synthesis (Figure 1a).

Figure 1b depicts the PL analysis of GO/Mn/Ch/FA-Brucine NCs. The excitations of the NCs occurred at 369.90, 433.98, and 480.42 nm. The PL spectrum provides information regarding the crystal mode, surface characteristics, and structural flaws of the NCs. The peaks at 369.90 nm suggest the recombination of free excitons. The green emission at the 433.98 nm peak can be because of the existence of interstitial oxygen vacancies. The green emission at 480.42 nm indicates that the NCs included a solitary ionized oxygen vacancy (Figure 1b).

The purity and crystalline nature of GO/Mn/Ch/FA-Brucine NCs were assessed through the XRD analysis

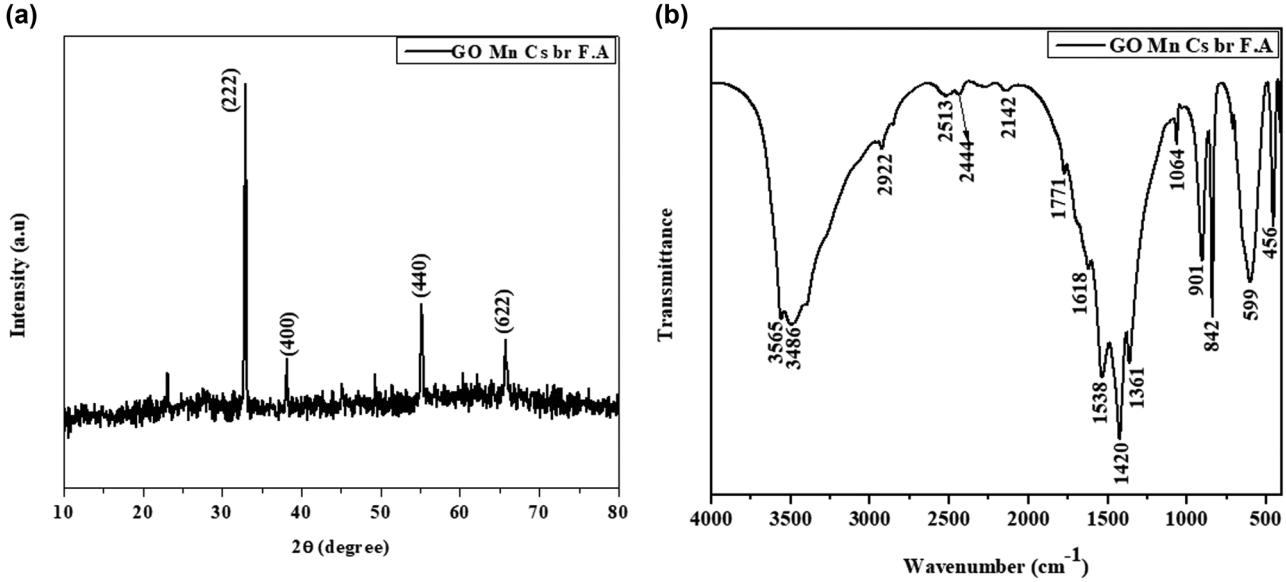

Figure 2: XRD and FT-IR analysis of the synthesized GO/Mn/Ch/FA-Brucine NCs. The peaks corresponding to the crystalline form of GO/Mn/Ch/FA-Brucine NCs were seen at specific crystallographic orientations, such as (222), (400), (440), and (622) (a). The FT-IR analysis revealed the occurrence of the specific functional groups present in the synthesized GO/Mn/Ch/FA-Brucine NCs (b).

(Figure 2a). The peaks corresponding to the crystalline form of the NCs were seen at specific crystallographic orientations, such as (222), (400), (440), and (622) (Figure 2a).

The FT-IR study was conducted to analyze the specific functional groups in GO/Mn/Ch/FA-Brucine NCs. The outcomes of this study are depicted in Figure 2b. The FT-IR spectra of the GO/Mn/Ch/FA-Brucine NCs exhibited a diverse range of peaks distributed across different frequencies. Major peaks at 3,565 and 3,468 cm^{-1} may be due to the vibrational band arising from the stretching motion of the O–H bond. The peaks at 2,922, 2,513, 2,444, and 2,142 cm^{-1} indicate the hydroxyl stretching. The peaks at 1,771, 1,618, 1,538, 1,420, 1,361, and 1,064 cm^{-1} correspond to the bending vibrations of C–H and C–O bonds, respectively. The peaks at 901, 842, 599, and 456 cm^{-1} correspond to H–O bonds.

The structure and appearance of the NCs were assessed using SEM, whereas their elemental constituents were determined using EDX spectroscopic analysis. The SEM microphotographs (Figure 3a) revealed that the NCs exhibited tetragonal and agglomerated morphological characteristics. The EDX analysis on the NCs revealed distinct peaks, suggesting the existence of carbon, nitrogen, and oxygen elements (Figure 3b).

The TEM images of GO/Mn/Ch/FA-Brucine NCs (Figure 4) revealed that the NCs exhibited cuboidal morphologies with an average diameter of 63 nm. The crystallization of the NCs was confirmed by examining selected area electron diffraction (SAED) patterns.

The DLS analysis was used to investigate the dispersion and particle size of the NCs (Figure 5), and the results revealed a reduced dispersion pattern with an average particle size of 136.20 nm.

3.2 Antimicrobial effects of GO/Mn/Ch/FA-Brucine NCs

The well diffusion technique was used to analyze the antimicrobial effects of GO/Mn/Ch/FA-Brucine NCs against several pathogens, including *B. subtilis*, *S. aureus*, *P. vulgaris*, *K. pneumoniae*,

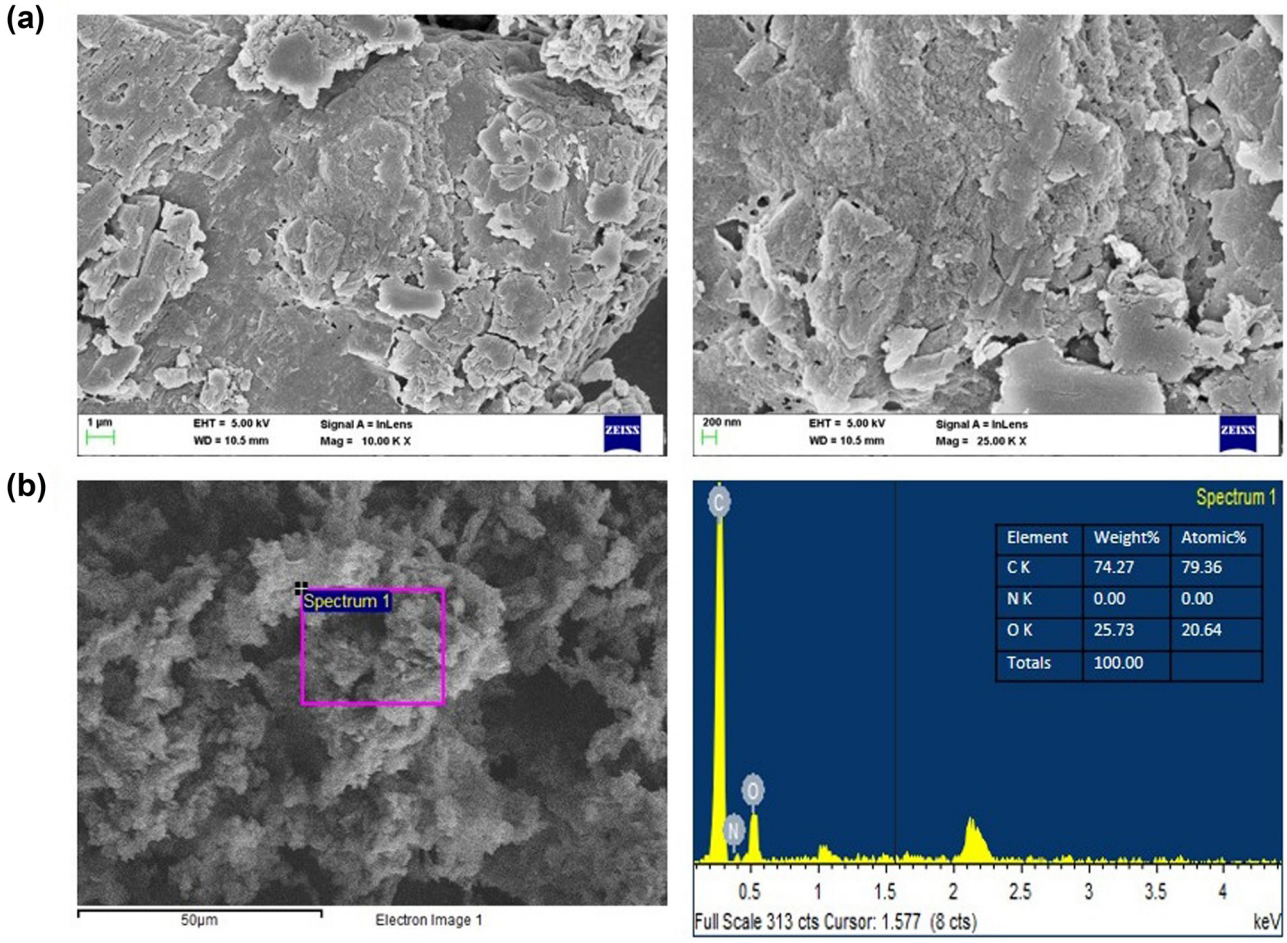

Figure 3: SEM and EDX analysis of the synthesized GO/Mn/Ch/FA-Brucine NCs. The SEM images revealed that the GO/Mn/Ch/FA-Brucine NCs exhibited tetragonal and agglomerated morphological characteristics (a). EDX analysis of the GO/Mn/Ch/FA-Brucine NCs showed different peaks, which suggests that carbon, nitrogen, and oxygen are present (b).

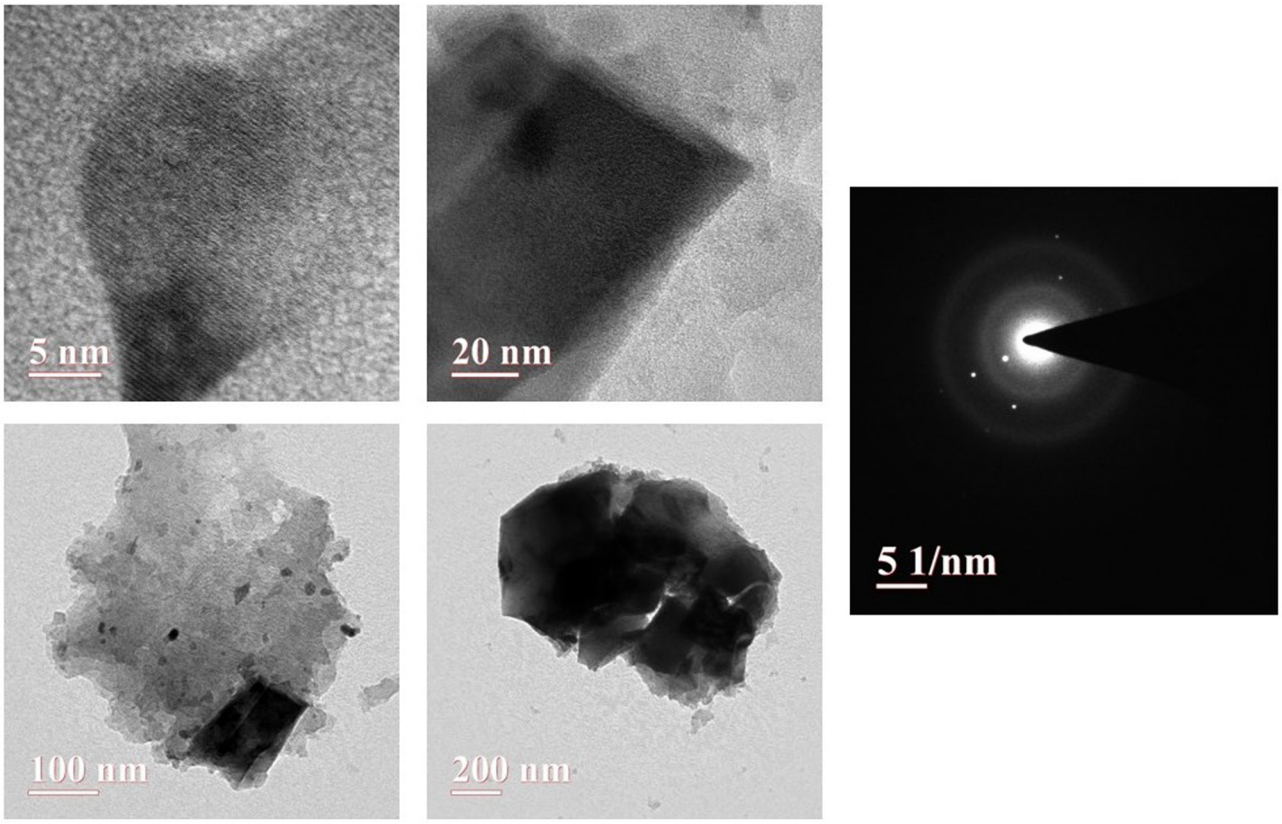

Figure 4: TEM analysis of the synthesized GO/Mn/Ch/FA-Brucine NCs. The TEM images revealed that the fabricated GO/Mn/Ch/FA-Brucine NCs exhibited cuboidal morphologies with an average diameter of 63 nm. The validation of the crystallization of the GO/Mn/Ch/FA-Brucine NCs was confirmed through the examination of the SAED patterns.

S. pneumoniae, *E. coli*, and *C. albicans* (Figure 6). The NC treatment with varying concentrations exhibited remarkable antimicrobial efficacy against all examined pathogens, corroborating the results observed with amoxicillin. The growth of several pathogens, particularly *E. coli*, *S. aureus*, and *C. albicans*, was effectively suppressed by GO/Mn/Ch/FA-Brucine NCs. This suppression was demonstrated by the highest inhibition zone observed in these pathogens when exposed to the NCs (Figure 7).

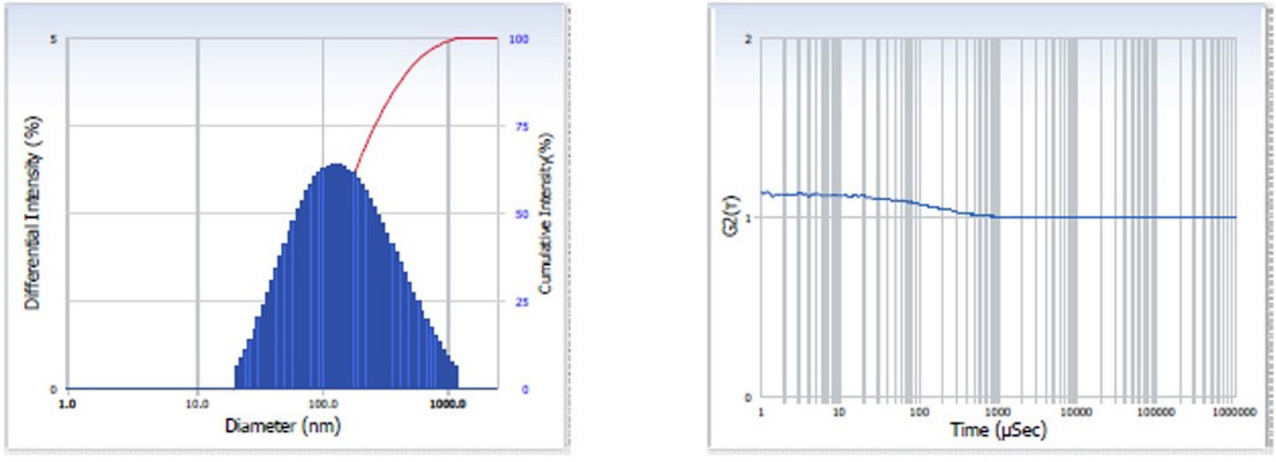

Figure 5: DLS analysis of the synthesized GO/Mn/Ch/FA-Brucine NCs. The findings from the DLS study revealed a reduced dispersion pattern with an average particle size of 136.20 nm.

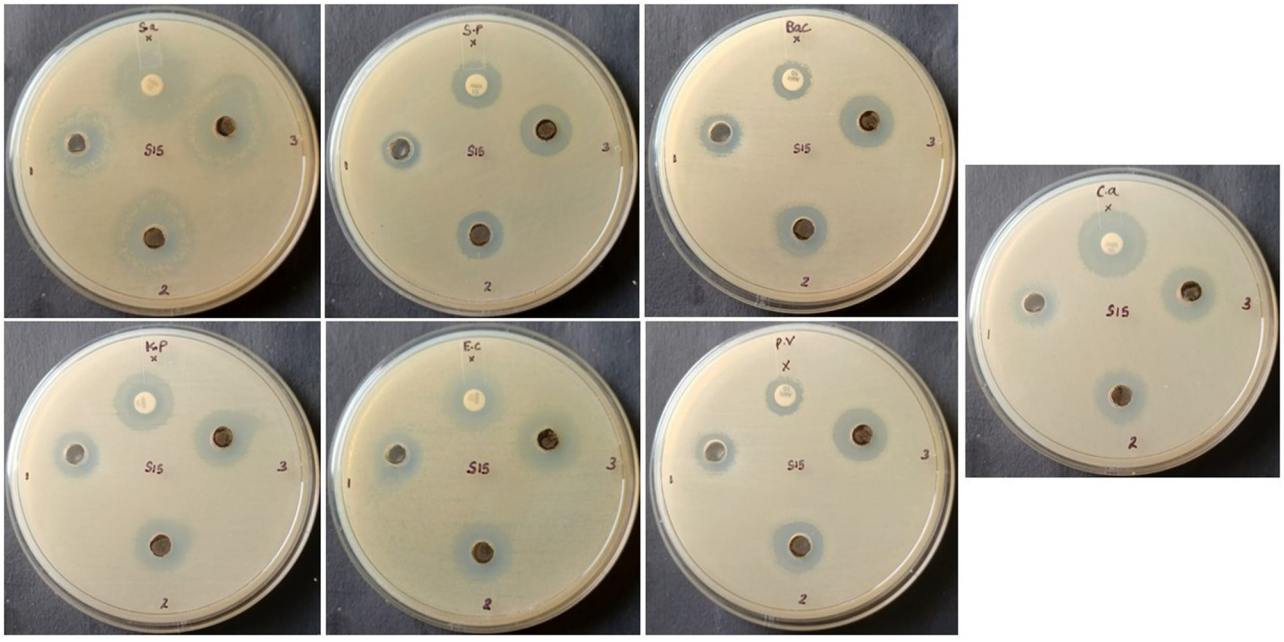

Figure 6: Antimicrobial activity of the synthesized GO/Mn/Ch/FA-Brucine NCs. The treatment of various concentrations of the synthesized GO/Mn/Ch/FA-Brucine NCs effectively decreased the growth of tested pathogens, particularly *E. coli*, *S. aureus*, and *C. albicans*, which were more sensitive to the NCs.

3.3 Effect of GO/Mn/Ch/FA-Brucine NCs on the HepG2 and Hep3B cell viability

The cytotoxic effects of GO/Mn/Ch/FA-Brucine NCs on HepG2 and HepB3 cells are shown in Figure 8. The NC treatment with varying doses (2, 4, 6, 8, 10, and 12 µg) considerably decreased the proliferative capacity of HepG2 and Hep3B cells. At higher concentrations of GO/Mn/Ch/FA-Brucine NCs, cell viability was markedly decreased in HepG2 cells than in Hep3B cells. The IC50 value of GO/Mn/Ch/FA-Brucine NCs for HepG2 cells was 6 µg; therefore, 6 and 8 µg were selected as IC50 and high doses of the NC for further assays, respectively.

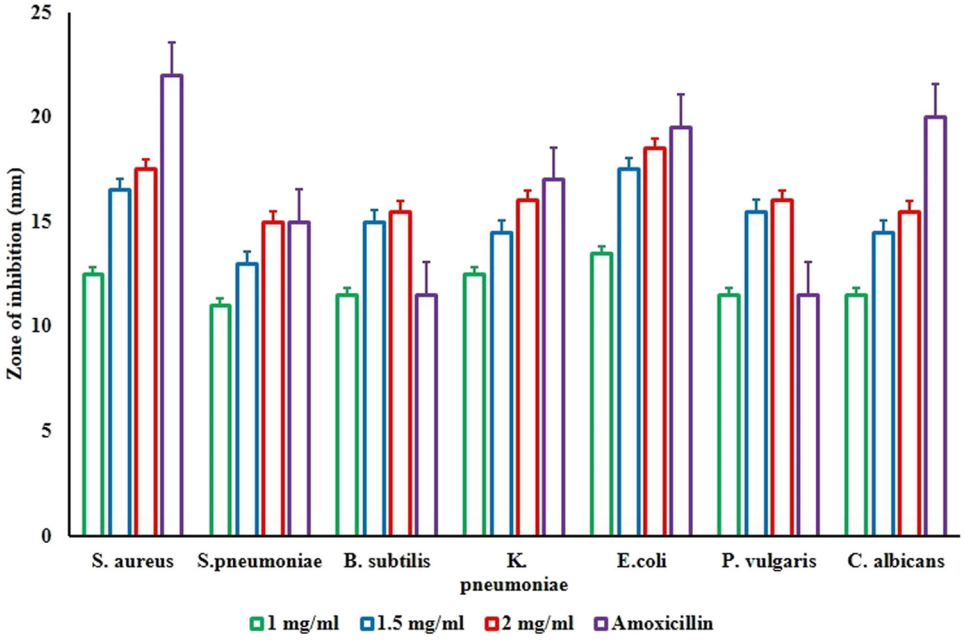

Figure 7: Antimicrobial activity of the synthesized GO/Mn/Ch/FA-Brucine NCs. The data were given as a mean ± SD of triplicates. The results were statistically studied by one-way ANOVA and DMRT assays using the GraphPad Prism software. Values not sharing common superscript and data were significantly different from control at $p < 0.01$.

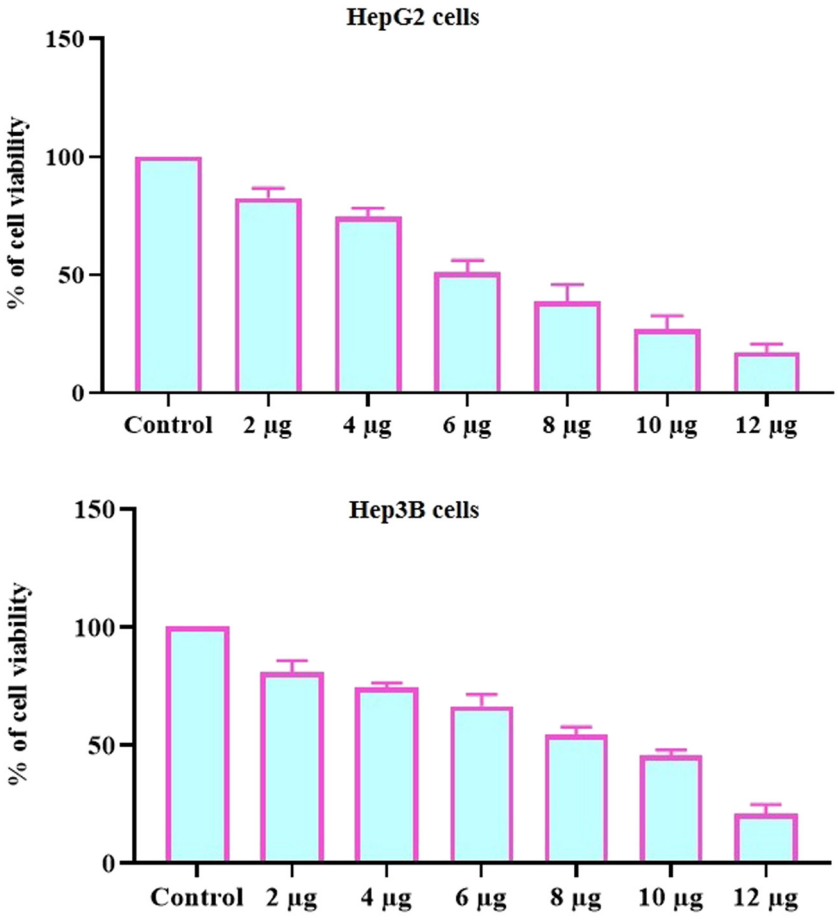

Figure 8: Effect of GO/Mn/Ch/FA-Brucine NCs on the viability of HepG2 and Hep3B cells. The data were given as a mean ± SD of triplicates. The results were statistically studied by one-way ANOVA and DMRT assays using the GraphPad Prism software. Values not sharing common superscript significantly differ from control at $p < 0.01$.

3.4 Effect of GO/Mn/Ch/FA-Brucine NCs on the apoptosis in HepG2 cells

The findings of the dual staining analysis of apoptotic cell death are indicated in Figure 9. The NC treatment at 6 and 8 µg resulted in more yellow and orange fluoresced cells, respectively, than the untreated cells. The green fluoresced cells in the control well represent normal viable cells, whereas the increased yellow and orange fluoresced cells in the NC-treated wells indicate the existence of more early and late apoptotic cells, respectively.

3.5 Effect of GO/Mn/Ch/FA-Brucine NCs on the oxidative and antioxidative biomarkers in HepG2 cells

The NC treatment on the levels of TBARS and antioxidants (GSH, CAT, and SOD) in HepG2 cells are depicted in Figure 10. The NC treatment of HepG2 cells at 6 and 8 µg considerably increased the TBARS levels. Furthermore, the NCs at 6 and 8 µg effectively reduced the GSH, CAT, and SOD levels in HepG2 cells. There was a considerable reduction in antioxidants and an upsurge in oxidative stress upon the NC treatment with HepG2 cells (Figure 10).

3.6 Effect of GO/Mn/Ch/FA-Brucine NCs on the inflammatory marker levels in the HepG2 cells

The levels of inflammatory markers (TNF-α, NF-κB, COX-2, and IL-6) were evaluated in untreated and NC-treated HepG2 cells (Figure 11). Compared with the control cells, the NC treatment at 6 and 8 µg significantly decreased the levels of TNF-α, NF-κB, COX-2, and IL-6 in HepG2 cells.

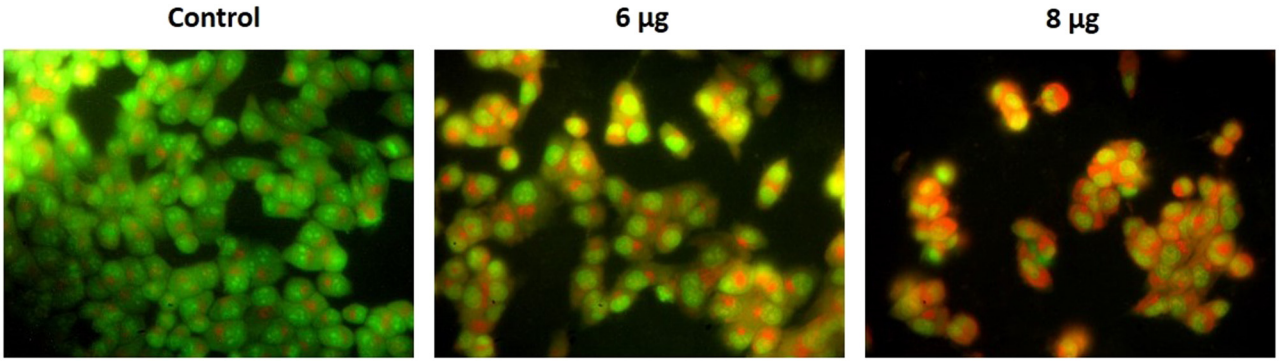

Figure 9: Effect of GO/Mn/Ch/FA-Brucine NCs on the apoptosis in the HepG2 cells. The GO/Mn/Ch/FA-Brucine NCs-treated HepG2 cells demonstrated a higher number of cells with yellow and orange fluorescence, which represent the occurrence of apoptotic events. Magnification: 20×; scale bar: 50 µm.

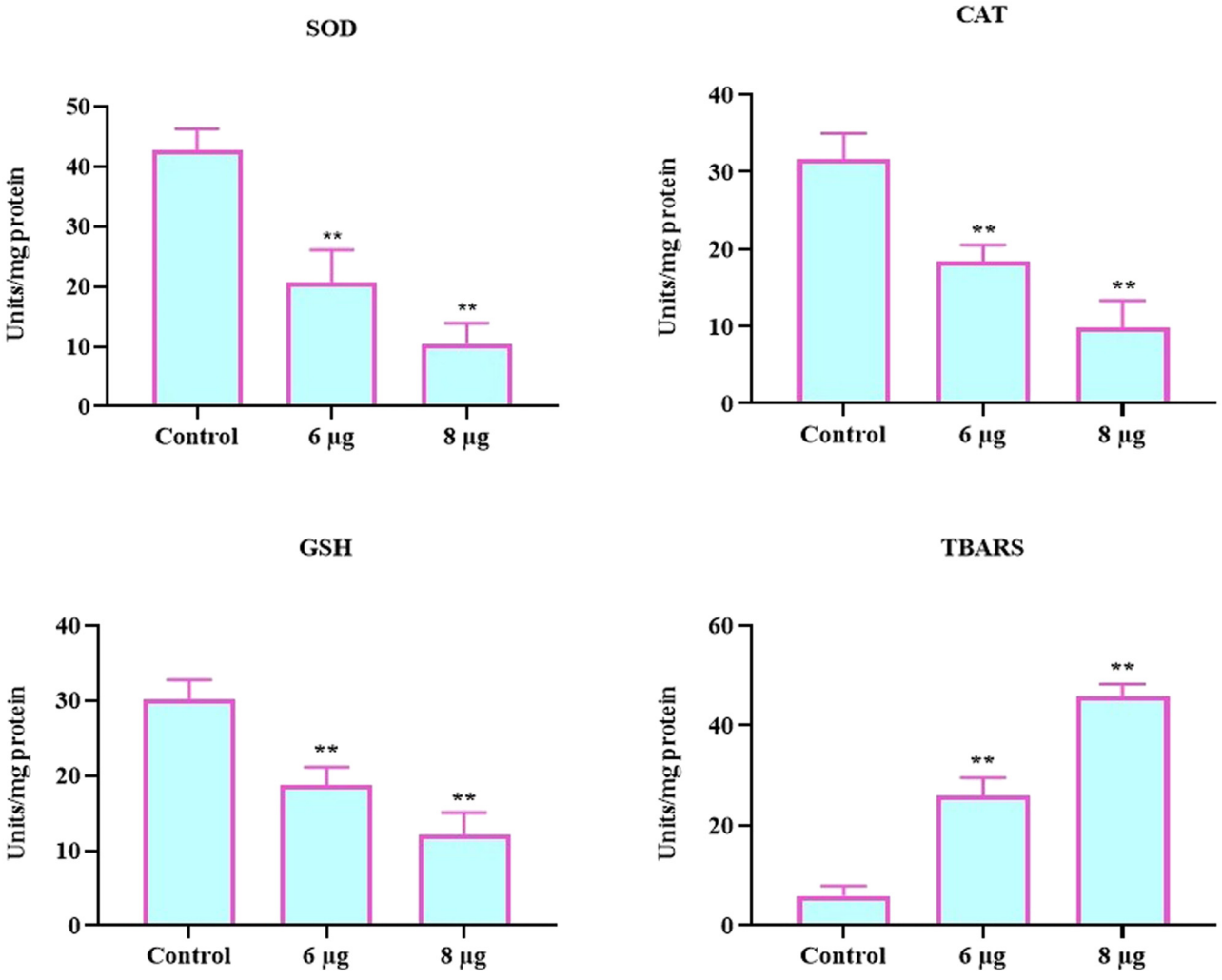

Figure 10: Effect of GO/Mn/Ch/FA-Brucine NCs on the oxidative and antioxidative biomarkers in the HepG2 cells. The data were given as a mean ± SD of triplicates. The results were statistically studied by one-way ANOVA and DMRT assays using the GraphPad Prism software. "**" denotes that values are significantly different from control at $p < 0.01$.

4 Discussion

Nanomedicine employs nanomaterials and nanotechnology to develop novel pharmaceuticals and delivery mechanisms with the aim of enhancing the effectiveness of current therapeutic approaches. Nanomedicines possess several advantageous characteristics in the field of cancer research, including their diminutive size and remarkable drug release profiles. These attributes give them significant capacity to address the limitations associated with existing chemotherapeutic treatments. Significantly, nanomaterials have the ability to enhance the effectiveness of chemotherapeutic drug-loaded therapies and mitigate the adverse effects of these drugs by accurate targeting [23]. There is evidence supporting the enhanced therapeutic effectiveness and reduced adverse effects of anticancer treatments through the utilization of nanomaterial-based drug delivery systems [24]. Various challenges, such as limited ability to penetrate tumors, non-specific accumulation in tissues, premature release of drugs into tissues, and uncontrolled drug release at the intended site, can be addressed through the utilization of drug delivery systems that have been effectively studied in human and animal models [25].

Chemotherapeutic treatments involve the administration of drugs through injection or ingestion, which exert their effects throughout the body. Nevertheless, significant efforts have been dedicated by the pharmaceutical sector toward the advancement of methodologies that enhance the selectivity of anti-cancer medications, thereby minimizing the adverse effects associated with systemic

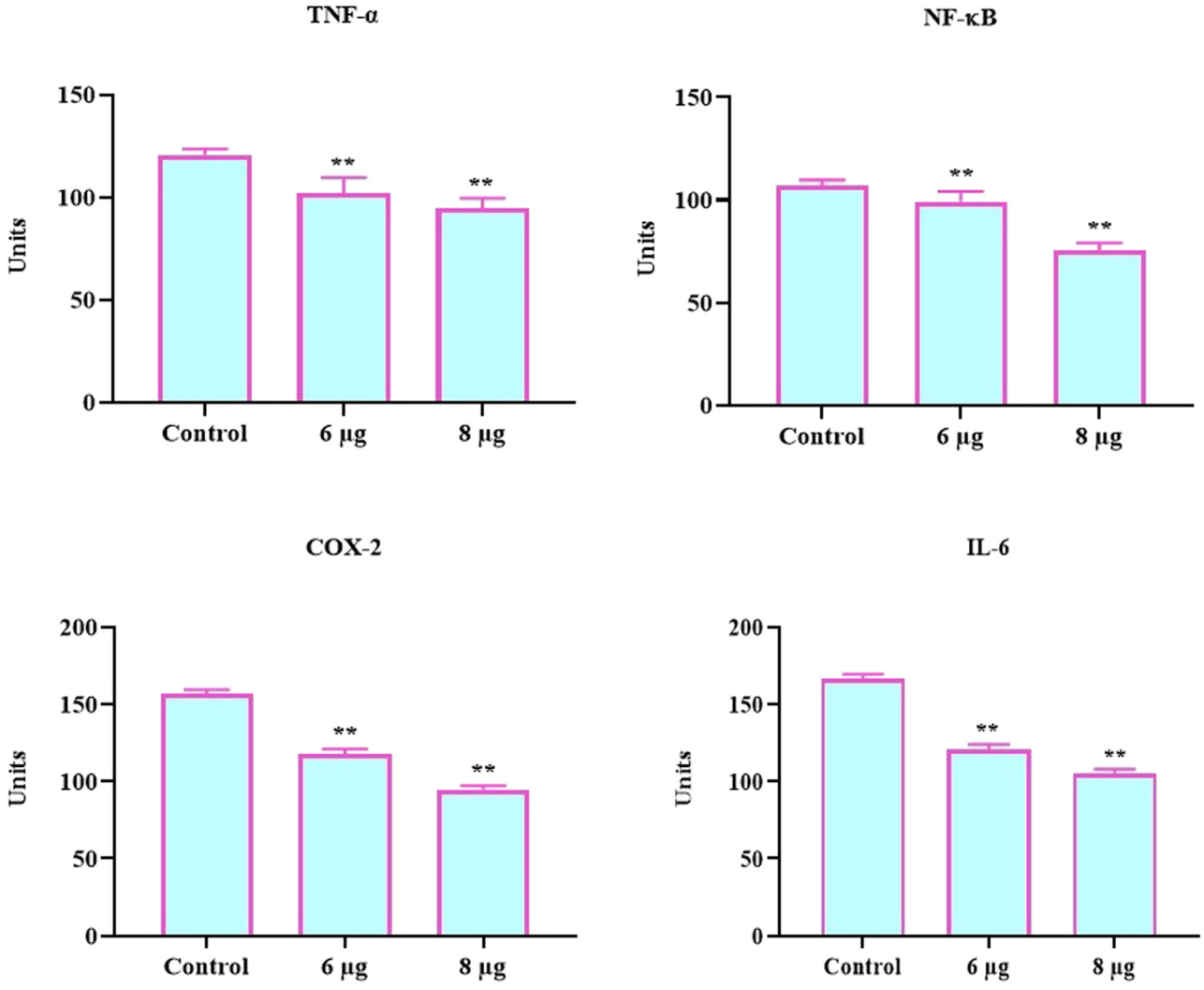

Figure 11: Effect of GO/Mn/Ch/FA-Brucine NCs on the inflammatory marker levels in the HepG2 cells. The data were given as a mean ± SD of triplicates. The results were statistically studied by one-way ANOVA and DMRT assays using the GraphPad Prism software. "**" denotes that values are significantly different from control at $p < 0.01$.

therapy [26]. In the present scenario, the functionalization of nanocarrier surfaces has emerged as a feasible option to enhance the efficiency of drug delivery to targeted locations and minimize the dosage of delivered pharmaceuticals. Promising outcomes were achieved by the utilization of screening tests conducted both *in vitro* and *in vivo*, employing nanomaterials that were functionalized with several active constituents such as Ch and FA. FA is a chemical that has a strong binding affinity for tumor cells, thereby facilitating the uptake of nanomaterials [27].

The potential for reduced toxicity and wide-ranging applicability makes it a promising agent for drug delivery and anticancer purposes [28]. The evaluation of the toxicity of a drug candidate is highly recommended in the clinical environment of cancer treatment due to its time-consuming and complex nature [29]. Therefore, in this study, the cytotoxicity of the synthesized GO/Mn/Ch/FA-Brucine NCs was evaluated against HepG2 and Hep3B cells. The findings of the MTT assay confirmed that the GO/Mn/Ch/FA-Brucine NCs treatment substantially diminished the growth of both HepG2 and Hep3B cells, which evidence the cytotoxicity of GO/Mn/Ch/FA-Brucine NCs to liver cancer cells.

Apoptosis, often known as programmed cell death, is of utmost importance to the cell cycle mechanisms and is characterized by nuclear fragmentation, cell shrinkage, mRNA degradation, DNA fragmentation, and the formation of membrane-bound protrusions known as blebs [30]. Apoptosis serves as the principal mechanism that plays a pivotal role in regulating cellular homeostasis by regulating cell growth and death, thereby preventing the development of uncontrolled cellular proliferation, commonly known as cancer [31]. The deregulation of apoptosis has profound implications for the growth of cancer. The variation between the rate of cell proliferation and cell death is widely recognized as a defining characteristic of malignant tumors [32]. Hence, it is imperative to maintain cellular homeostasis by balancing the rates of cell growth and cell death in order to support regular physiological functions. The development of novel therapeutic approaches that specifically target the apoptotic process in cancer treatment is a promising technique. The current results proved that treatment with synthesized GO/Mn/Ch/FA-Brucine NCs effectively induced apoptotic cell death in the HepG2 cells.

Cells undergoing apoptosis exhibit the formation of large vesicles, known as apoptotic bodies, which contain a distinct phospholipid known as phosphatidylserine. This phospholipid serves as a signaling molecule, effectively alerting adjacent cells, which is characterized as an early apoptotic mechanism. Late apoptosis is a state that is irreversible in nature and is distinguished by the full disaggregation of the cytoskeleton, permeation of the cell, and disintegration. The benefits of inducing apoptosis in cancer cells depend on the ability to prevent an inflammatory reactions [33]. Apoptotic bodies are generated as a result of the apoptotic process and are utilized by phagocytic cells, which play a crucial role in preventing cancer cell growth [34]. The findings of the dual staining assay revealed the occurrence of apoptotic cell death in the GO/Mn/Ch/FA-Brucine NCs-treated HepG2 cells with distinct morphological changes.

The metabolic level of tumor cells are higher than those of non-malignant cells, mostly due to their rapid proliferation rate. As a result, there was an increase in the generation of reactive oxygen species (ROS) and other free radicals. The significance of ROS in cancer cell metabolism is of utmost importance. Over accumulation of endogenous ROS can contribute to the growth of cancer by causing DNA impairments and cellular metabolic reprogramming [35]. The secretion of antioxidant enzymes from the cell was primarily aimed at restoring balance to the increased levels of ROS. The enzyme known as SOD is synthesized by normal cells and is capable of transforming superoxide radicals into hydrogen peroxide. The overexpression of SOD and CAT has the ability to provide protection to tumor cells against an excessive accumulation of ROS [36].

GSH is a crucial thiol-dependent antioxidant that plays a significant role in the protection against oxidative damage [37]. GSH is widely recognized as a pivotal regulator of cellular homeostasis as well as being involved in the processes of DNA replication and repair. A potential cause for the decrease in GSH concentration could be attributed to the process of glutathione oxidation, which occurs due to oxidative stress. The present study observed a substantial decrease in SOD, CAT, and GSH contents in HepG2 cells treated with GO/Mn/Ch/FA-Brucine NCs compared to the control. The outcomes of this work align with the observations made in NPs-treated cancer cell lines [38].

Inflammation is a fundamental part of the innate immune system, characterized by the mobilization and stimulation of immune cells along with the involvement of soluble mediators such as cytokines and chemokines. The inflammatory process has conventionally served as a primary mechanism of host defense against detrimental stimuli. In addition to its conventional function, inflammation has been found to have a significant association with cancer, as evidenced by comprehensive examinations of tumor transcriptomes. These analyses have unveiled a unique expression pattern of inflammatory cytokines and the presence of recruited immune cells in various types of tumors [39]. The current understanding in the scientific community is that inflammation serves a substantial role

in the tumor growth. The immune system plays a pivotal role in both facilitating and inhibiting various phases of tumor, and influencing the prognosis and treatment outcomes associated with cancer. Chronic inflammation, which precedes tumor growth and facilitates the development of cancer, has been identified as a contributing factor in some types of cancer [40].

Inflammatory cytokines like IL-6 and TNF-α promote the multiplication of cancer cells during the progression of a tumor. Additionally, many cytokines can act in opposition to the immune cells involved in anti-tumor responses [41]. TNF-α has been observed to facilitate the stimulation, differentiation, viability, or apoptosis of neoplastic cells within particular contexts. Furthermore, it has been observed that it exerts regulatory control over immunological and inflammatory responses [42]. The NF-κB transcription factors play pivotal roles in the process of carcinogenesis. The NF-κB pathway, when abnormally activated, has a crucial role in promoting tumor cell survival, inhibiting apoptosis, and promoting angiogenesis, hence facilitating the metastasis of malignancies to distant sites [43]. The inhibition of COX expression holds potential as a therapeutic approach for tumorigenesis. It was reported that inhibitors of COX exhibit cytotoxic effects on tumor cells by promoting apoptotic processes [44]. The results of this study highlighted that the GO/Mn/Ch/FA-Brucine NCs treatment effectively decreased the inflammatory markers in the HepG2 cells and facilitated apoptosis.

5 Conclusion

The present work showed that the GO/Mn/Ch/FA-Brucine NCs inhibited growth and induced apoptosis in liver cancer HepG2 cells. The NCs have shown significant effects in inhibiting viability, enhancing the cellular response to oxidative stress, and inducing apoptosis in the HepG2 cell line. The NCs also exhibited excellent antimicrobial activity. Therefore, our findings suggest that GO/Mn/Ch/FA-Brucine NCs are potential therapeutic agents to treat liver cancer. However, future research studies are needed to acquire a complete understanding of the precise molecular pathways underlying the anticancer properties of the NCs in the context of liver cancer.

Funding information: Authors state no funding involved.

Author contributions: Mohd Fahami Nur Azlina and Naiyer Shahzad: writing – original draft, writing – review and editing, formal analysis; Ibrahim M. Alanazi: writing – original draft, formal analysis; Ibrahim Abdel Aziz Ibrahim and Abdullah R. Alzahrani: supervision, conceptualization, visualization, and project administration; Palanisamy Arulselvan and Yusof Kamisah: writing – reviewing and editing; Imran Shahid and Nafeeza Mohd Ismail: methodology, formal analysis.

Conflict of interest: Authors state no conflict of interest.

Data availability statement: All data generated or analyzed during this study are included in this published article.

References

[1] Agnihotri A. Liver cancer deaths are expected to rise by more than 55% by 2040: research. Health-Hindustan times; 2022.
[2] Siegel RL, Miller KD, Wagle NS, Jemal A. Cancer statistics 2023. CA Cancer J Clin. 2023;73:17–48.
[3] Kirtonia A, Gala K, Fernandes SG, Pandya G, Pandey AK, Sethi G, et al. Repurposing of drugs: An attractive pharmacological strategy for cancer therapeutics. Semin Cancer Biol. 2021;68:258–78.
[4] Paskeh MDA, Ghadyani F, Hashemi M, Abbaspour A, Zabolian A, Javanshir S, et al. Biological impact and therapeutic perspective of targeting PI3K/Akt signaling in hepatocellular carcinoma: promises and challenges. Pharmacol Res. 2022;187:106553.
[5] Cassinotto C, Nogue E, Durand Q, Panaro F, Assenat E, Dohan A, et al. Life expectancy of patients with hepatocellular carcinoma according to the upfront treatment: a nationwide analysis. Diagn Interv Imaging. 2023;104:192–9.
[6] Dehshahri A, Ashrafizadeh M, Ghasemipour Afshar E, Pardakhty A, Mandegary A, Mohammadinejad R, et al. Topoisomerase inhibitors: pharmacology and emerging nanoscale delivery systems. Pharmacol Res. 2020;151:104551.
[7] Lodhi MS, Khan MT, Aftab S, Samra ZQ, Wang H, Wei DQ. A novel formulation of theranostic nanomedicine for targeting drug delivery to gastrointestinal tract cancer. Cancer Nanotechnol. 2021;12(1):1–27.
[8] Tang Z, Gao H, Chen X, Zhang Y, Li A, Wang G. Advanced multifunctional composite phase change materials based on photoresponsive materials. Nano Energy. 2021;80:105454.
[9] Herdiana Y, Wathoni N, Shamsuddin S, Joni IM, Muchtaridi M. Chitosan-based nanoparticles of targeted drug delivery system in breast cancer treatment. Polymers (Basel). 2021;13(11):1717.
[10] Tinajero-Díaz E, Salado-Leza D, Gonzalez C, Martínez Velázquez M, López Z, Bravo-Madrigal J, et al. Green metallic nanoparticles for cancer therapy: evaluation models and cancer applications. Pharmaceutics. 2021;13(10):1719.
[11] Lee J, Yim Y, Kim S, Choi M-H, Choi B-S, Lee Y, et al. In-depth investigation of the interaction between DNA and nano-sized graphene oxide. Carbon. 2016;97:92–988.
[12] Park J, Kim B, Han J, Oh J, Park S, Ryu S, et al. Graphene oxide flakes as a cellular adhesive: prevention of reactive oxygen species mediated death of implanted cells for cardiac repair. ACS Nano. 2015;9(5):4987–99.

[13] Xu Z, Wang S, Li Y, Wang M, Shi P, Huang X. Covalent functionalization of graphene oxide with biocompatible poly(ethyleneglycol) for delivery of paclitaxel. ACS Appl Mater Interfaces. 2014;6:17268–76.
[14] Cao L, Zhang F, Wang Q, Wu X. Fabrication of chitosan/graphene oxide polymer nanofiber and its biocompatiility for cartilage tissue engineering. Mater Sci Eng C. 2017;79:697–701.
[15] Nogueira E, Freitas J, Loureiro A, Nogueira P, Gomes AC, Preto A, et al. Neutral PEGlated liposomal formulation for efficient folate-mediated delivery of MCL1 siRNA to activated macrophages. Colloid Surf B. 2017;155:459–65.
[16] Lu L, Huang R, Wu Y, Jin JM, Chen HZ, Zhang LJ, et al. Brucine: a review of phytochemistry, pharmacology, and toxicology. Fron Pharmacol. 2020;11:377.
[17] Li M, Li P, Zhang M, Ma F. Brucine suppresses breast cancer metastasis via inhibiting epithelial mesenchymal transition and matrix metalloproteinases expressions. Chin J Integr Med. 2018;24:40–6.
[18] Shi X, Zhu M, Kang Y, Yang T, Chen X, Zhang Y. Wnt/β-catenin signaling pathway is involved in regulating the migration by an effective natural compound brucine in LoVo cells. Phytomedicine. 2018;46:85–92.
[19] Yan W, Zeng Z, Qin F, Xu J, Liao Z, Ouyang M. Effects of brucine on mitochondrial apoptosis and expression of HSP70 in prostate cancer cells. Transl Cancer Res. 2022;11(3):500–7.
[20] CLSI, Performance Standards for Antimicrobial Disk Susceptibility Tests, Approved Standard, 7th ed., CLSI document M02-A11. Clinical and Laboratory Standards Institute, 950 West Valley Road, Suite 2500, Wayne, Pennsylvania 19087, USA; 2012.
[21] Mosmann T. Rapid colorimetric assay for cellular growth and survival: application to proliferation and cytotoxicity assays. J Immunol Methods. 1983;65(1–2):55–63.
[22] Taatjes DJ, Wadsworth MP, Zaman AK, Schneider DJ, Sobel BE. A novel dual staining method for identification of apoptotic cells reveals a modest apoptotic response in infarcted mouse myocardium. Histochem Cell Biol. 2007;128(3):275–83.
[23] Thakur AK, Chellappan DK, Dua K, Mehta M, Satija S, Singh I. Patented therapeutic drug delivery strategies for targeting pulmonary diseases. Expert Opin Ther Pat. 2020;30(5):375–87.
[24] Sharma A, Shambhwani D, Pandey S, Singh J, Lalhlenmawia H, Kumarasamy M, et al. Advances in lung cancer treatment using nanomedicines. ACS Omega. 2022;8(1):10–41.
[25] Gai S, Yang G, Yang P, He F, Lin J, Jin D, et al. Recent advances in functional nanomaterials for light-triggered cancer therapy. Nano Today. 2018;19:146–87.
[26] Thapa RK, Choi Y, Jeong JH, Youn YS, Choi HG, Yong CS, et al. Folate-mediated targeted delivery of combination chemoterapeutics loaded reduced graphene oxide for synergistic chemophotothermal therapy of cancer. Pharm Res. 2016;33:2816–27.
[27] Marino FZ, Ronchi A, Accardo M, Franco R. Detection of folate receptorpositive circulating tumor cells by ligand-targeted polymerase chain reaction in non-small cell lung cancer patients. J Thorac Dis. 2016;8:1437–9.
[28] Khursheed R, Dua K, Vishwas S, Gulati M, Jha NK, Aldhafeeri GM, et al. Biomedical applications of metallic nanoparticles in cancer: current status and future perspectives. Biomed Pharmacother. 2022;150:112951.
[29] Lin L, Cheng K, Xie Z, Chen C, Chen L, Huang Y, et al. Purification and characterization a polysaccharide from *Hedyotis diffusa* and its apoptosis inducing activity toward human lung cancer cell line A549. Int J Biol Macromol. 2019;122:64–71.
[30] Morana O, Wood W, Gregory CD. The apoptosis paradox in cancer. Int J Mol Sci. 2022;23:1328.
[31] Yamaguchi Y, Shiraki K, Fuke H, Inoue T, Miyashita K, Yamanaka Y, et al. Targeting of X-linked inhibitor of apoptosis protein or Survivin by short interfering RNAs sensitises hepatoma cells to TNF-related apoptosis-inducing ligand- and chemotherapeutic agent-induced cell death. Oncol Rep. 2005;12:1211–316.
[32] Giorgi C, Romagnoli A, Pinton P, Rizzuto R. Ca2 + signaling, mitochondria and cell death. Curr Mol Med. 2008;8(2):119–30.
[33] Elmore S. Apoptosis: a review of programmed cell death. Toxicol Pathol. 2007;35(4):495–516.
[34] Kroemer G, El-Deiry WS, Golstein P, Peter ME, Vaux D, Vandenabeele P, et al. Classification of cell death: recommendations of the nomenclature committee on cell death. Cell Death Differ. 2005;12:1463–7.
[35] Panieri E, Santoro MM. Ros homeostasis and metabolism: a dangerous liason in cancer cells. Cell Death Dis. 2016;7:e2253.
[36] Glorieux C, Calderon PB. Catalase down-regulation in cancer cells exposed to arsenic trioxide is involved in their increased sensitivity to a pro-oxidant treatment. Cancer Cell Int. 2018;18:24.
[37] Kretowski R, Jabłońska-Trypuć A, Cechowska-Pasko M. The preliminary study on the proapoptotic effect of reduced graphene oxide in breast cancer cell lines. Int J Mol Sci. 2021;22:12593.
[38] Shiny P, Mukherjee A, Chandrasekaran N. Haemocompatibility assessment of synthesised platinum nanoparticles and its implication in biology. Bioproc Biosyst Eng. 2014;37(6):991–7.
[39] Binnewies M, Roberts EW, Kersten K, Chan V, Fearon DF, Merad M, et al. Understanding the tumor immune microenvironment (TIME) for effective therapy. Nat Med. 2018;24:541–50.
[40] Greten FR, Grivennikov SI. Inflammation and cancer: triggers, mechanisms, and consequences. Immunity. 2019;51:27–41.
[41] Suarez-Carmona M, Lesage J, Cataldo D, Gilles C. EMT and inflammation: Inseparable actors of cancer progression. Mol Oncol. 2017;11:805–23.
[42] Desplat-Jégo S, Burkly L, Putterman C. Targeting TNF and its family members in autoimmune/inflammatory disease. Mediators Inflamm. 2014;2014:628748.
[43] Xia Y, Shen S, Verma IM. NF-κB, an active player in human cancers. Cancer Immunol Res. 2014;2:823–30.
[44] Szweda M, Rychlik A, Babińska I, Pomianowski A. Cyclooxygenase-2 as a biomarker with diagnostic, therapeutic, prognostic, and predictive relevance in small animal oncology. J Vet Res. 2020 Mar;64(1):151–60.